Monthly Notices
of the
ROYAL ASTRONOMICAL SOCIETY

MNRAS **441,** 289–303 (2014) doi:10.1093/mnras/stu538

The supernova CSS121015:004244+132827: a clue for understanding superluminous supernovae

S. Benetti,[1★] M. Nicholl,[2] E. Cappellaro,[1] A. Pastorello,[1] S. J. Smartt,[2] N. Elias-Rosa,[1,3] A. J. Drake,[4] L. Tomasella,[1] M. Turatto,[1] A. Harutyunyan,[5] S. Taubenberger,[6] S. Hachinger,[1,7] A. Morales-Garoffolo,[3] T.-W. Chen,[2] S. G. Djorgovski,[4] M. Fraser,[2] A. Gal-Yam,[8] C. Inserra,[2] P. Mazzali,[1,9] M. L. Pumo,[1] J. Sollerman,[10,11] S. Valenti,[12,13] D. R. Young,[2] M. Dennefeld,[14] L. Le Guillou,[15] M. Fleury[15] and P.-F. Léget[16]

[1]*INAF – Osservatorio Astronomico di Padova, vicolo dell'Osservatorio 5, I-35122 Padova, Italy*
[2]*Queen's University Belfast, Belfast BT7 1NN, UK*
[3]*Institut de Ciències de l'Espai (CSIC-IEEC), Facultat de Ciències, Campus UAB, E-08193 Bellaterra, Spain*
[4]*California Institute of Technology, 1200 E. California Blvd., CA 91225, USA*
[5]*Telescopio Nazionale Galileo, Fundación Galileo Galilei – INAF, Rambla José Ana Fernández Pérez, 7, E-38712 Breña Baja, TF, Spain*
[6]*Max-Planck-Institut für Astrophysik, Karl Schwarzschild Str. 1, D-85741 Garching bei München, Germany*
[7]*Institut für Theoretische Physik und Astrophysik, Universität Würzburg, D-97074 Würzburg, Germany*
[8]*Benoziyo Center for Astrophysics, Weizmann Institute of Science, Rehovot 76100, Israel*
[9]*Liverpool John Moores, Liverpool Science Park, IC2 building, 146 Brownlow Hill, Liverpool L3 5RF, UK*
[10]*Department of Astronomy, AlbaNova Science Center, Stockholm University, SE-106 91 Stockholm, Sweden*
[11]*The Oskar Klein Centre, AlbaNova, SE-106 91 Stockholm, Sweden*
[12]*Department of Physics, University of California, Santa Barbara, Broida Hall, Mail Code 9530, Santa Barbara, CA 93106-9530, USA*
[13]*Las Cumbres Observatory, Global Telescope Network, 6740 Cortona Drive Suite 102, Goleta, CA 93117, USA*
[14]*CNRS, Institut dAstrophysique de Paris (IAP) and University P. et M. Curie (Paris 6), 98bis, Boulevard Arago F-75014 Paris, France*
[15]*UPMC Univ. Paris 06, UMR 7585, Laboratoire de Physique Nucleaire et des Hautes Energies (LPNHE), F-75005 Paris, France*
[16]*Clermont Université, Université Blaise Pascal, CNRS/IN2P3, Laboratoire de Physique Corpusculaire, BP 10448, F-63000 CLERMONT-FERRAND, France*

Accepted 2014 March 17. Received 2014 March 17; in original form 2013 October 4

ABSTRACT

We present optical photometry and spectra of the superluminous Type II/IIn supernova (SN) CSS121015:004244+132827 ($z = 0.2868$) spanning epochs from −30 d (rest frame) to more than 200 d after maximum. CSS121015 is one of the more luminous SNe ever found and one of the best observed. The photometric evolution is characterized by a relatively fast rise to maximum (∼40 d in the SN rest frame), and by a linear post-maximum decline. The light curve shows no sign of a break to an exponential tail. A broad Hα is first detected at ∼+40 d (rest frame). Narrow, barely resolved Balmer and [O III] 5007 Å lines, with decreasing strength, are visible along the entire spectral evolution. The spectra are very similar to other superluminous supernovae (SLSNe) with hydrogen in their spectrum, and also to SN 2005gj, sometimes considered Type Ia interacting with H-rich circumstellar medium. The spectra are also similar to a subsample of H-deficient SLSNe. We propose that the properties of CSS121015 are consistent with the interaction of the ejecta with a massive, extended, opaque shell, lost by the progenitor decades before the final explosion, although a magnetar-powered model cannot be excluded. Based on the similarity of CSS121015 with other SLSNe (with and without H), we suggest that the shocked-shell scenario should be seriously considered as a plausible model for both types of SLSN.

Key words: supernovae: general – supernovae: individual: CSS121015:004244+132827.

1 INTRODUCTION

Supernovae (SNe), the dramatic and violent endpoints of stellar evolution, lie at the heart of some of the most important problems

★ E-mail: stefano.benetti@oapd.inaf.it

of modern astrophysics. New observational evidence, largely from extensive transient searches (e.g. the Catalina Real-time Transient Survey, the Palomar Transient Factory, Pan-STARRS1, La Silla Quest, etc., Drake et al. 2009; Law et al. 2009; Tonry et al. 2012; Baltay et al. 2013, respectively), is shedding new light both at the bright and faint ends of the SN luminosity distribution. In particular, a number of exceptionally luminous objects (superluminous supernovae, SLSNe) are challenging our existing theoretical picture of the late evolution and explosion of massive stars. It is crucial to understand the nature of these events because, with the next generation of instruments, they may be used to probe star formation and chemical enrichment in the very early Universe (Pop III stars; e.g. Whalen et al. 2013).

While SLSNe are picked out by simple measurement of the total luminosity (Gal-Yam 2012), there is a large diversity in their spectral types and light-curve evolution. By volume, they are rare (Quimby et al. 2013), and most have been related to massive stars of some sort. However, whether or not their rarity points to an origin at the top end of the mass function, or to some other characteristics of the progenitor (e.g. extremely low metallicity), is not known. Some SLSNe show clear spectral signatures of hydrogen – usually relatively narrow emission lines, leading to the classification as Type IIn events (e.g. Smith et al. 2007). In only one case (SN 2008es), H shows very broad emission features (Gezari et al. 2009; Miller et al. 2009). Finally, there appears to be a class of SLSNe that do not show H, and spectroscopically evolve to resemble stripped-envelope Type Ic SNe (e.g. Pastorello et al. 2010b; Quimby et al. 2011). These have been termed SLSNe-I by Gal-Yam (2012) and superluminous Type Ic SNe by Inserra et al. (2013). Originally classified as SLSNe by the first secure redshift determinations, they were shown to evolve spectroscopically into Type Ic-like SNe on very long time-scales by Pastorello et al. (2010b). They were discovered up to redshifts ∼1 in the Pan-STARRS1 Medium Deep Survey (Chomiuk et al. 2011), and a significant effort has been invested to characterize them retrospectively in ongoing surveys (Barbary et al. 2009; Leloudas et al. 2012). Cooke et al. (2012) and Howell et al. (2013) extended the discovery of SLSNe up to redshift >3.9.

It has been claimed that some of these SLSNe are powered by the radioactive decay of large amounts of ^{56}Ni, and are therefore the observational counterparts of the long-sought pair-instability SNe. These have even been proposed as a class named 'SLSN-R' (Gal-Yam 2012). The first example is the luminous and slowly declining SN 2007bi (Gal-Yam et al. 2009), although Young et al. (2010) suggested that a standard iron-core-collapse origin could not be ruled out (see also Moriya et al. 2013a), while Dessart et al. (2012) suggested that energy input from the spin-down of a newly formed magnetar powers the luminosity, instead of radioactive decay. Pair-instability SNe are predicted by stellar evolution theory to terminate the lives of stars with mass $>140\,M_\odot$ which have low enough mass-loss rates to retain a large CO core. However, their existence in the local Universe is not settled, since the observed properties of SLSNe can be explained by different physical processes, including magnetar spin-down (Kasen & Bildsten 2010; Woosley 2010; Dessart et al. 2012; Inserra et al. 2013; Nicholl et al. 2013), the accretion on to a proto-neutron star or a black hole (Dexter & Kasen 2013), or interaction of the ejecta with circumstellar material (Blinnikov & Sorokina 2010; Chevalier & Irwin 2011; Ginzburg & Balberg 2012; Moriya et al. 2013a,b,c).

The interaction of the ejecta with circumstellar medium (CSM) is seemingly a frequent phenomenon in massive star explosions, with a number of luminous transients already related to the violent shocks formed when multiple shells collide. This is the case for other kinds of outbursts that can compete with SNe in luminosities and expansion velocities (SN impostors; Van Dyk et al. 2000; Maund et al. 2006; Smith et al. 2011) even if the star survives the event. Eruptive mass-loss can build up a dense CSM around a massive star. When the star eventually explodes, the high-velocity ejecta impacts the dense CSM, converting part of its kinetic energy into radiation. The transient becomes very luminous, with a luminosity evolution modulated by the density profile of the CSM. When this mechanism is at work, it can easily outshine all other radiation sources – making it difficult, if not impossible, to identify the explosion mechanism or even to assess whether an underlying SN has occurred, as in the spectacular case of SN 2009ip (Fraser et al. 2013a; Margutti et al. 2014; Mauerhan et al. 2013; Pastorello et al. 2013, and references therein).

This potential for extreme brightness makes ejecta–CSM interaction an appealing physical scenario to explain SNe with unusually high luminosities (Chevalier & Irwin 2011; Ginzburg & Balberg 2012). This interpretation has been adopted for H-rich SLSNe, such as SN 2008es (Gezari et al. 2009; Miller et al. 2009), and may also be relevant to H-deprived transients (see e.g. Chatzopoulos et al. 2013, and references therein). In fact, very recently Ben-Ami et al. (2014) presented a case of a Type Ic SN whose ejecta started to interact with a massive, hydrogen-free ($\sim 3\,M_\odot$) CSM.

In this paper, we report on observations of a new event that appears to support the ejecta–CSM interpretation. CSS121015:004244+132827 (CSS121015 from here on) was first detected by Catalina Real-time Transient Survey (CRTS) on 2012 September 15, at a V magnitude of ∼20.0, as announced by Drake et al. (2012). They also reported that a spectrum taken with Palomar 5 m Telescope + double spectrograph (DBSP) on October 15 UT showed a very blue continuum with no clear emission features, resembling the early spectra of other luminous Type I SNe detected by CRTS. A follow-up spectroscopic observation by Tomasella et al. (2012), obtained with the Asiago 1.82 m Copernico Telescope + Asiago Faint Object Spectrograph and Camera (AFOSC), confirmed the very blue, featureless continuum, but also allowed the detection of faint, narrow Balmer emissions from the system. A redshift of ∼0.286 was hence derived, making CSS121015 extremely luminous (∼−22.5). The spectral appearance was that of a stripped-envelope SN such as those discussed in Quimby et al. (2011) and Pastorello et al. (2010b). After this classification, we began an extensive follow-up campaign for CSS121015 in the optical domain, within the frameworks of the Asiago-TNG Supernova follow-up campaign[1] and the Public ESO Spectroscopic Survey of Transient Objects (PESSTO).[2] In this paper, we present the results of this monitoring campaign and discuss the implications for the SLSN scenarios.

2 REDDENING AND DISTANCE OF CSS121015 AND ITS HOST GALAXY

The host of CSS121015 is a faint galaxy, barely visible in Sloan images (SDSS DR9[3]; Eisenstein et al. 2011). Using our deeper r-band frame (see Table 3), we measured an apparent magnitude of $r \sim 23.0$ for the parent galaxy.

The Galactic reddening towards CSS121015, $A_B = 0.314$, was taken from the recalibrated infrared-based dust map of Schlafly & Finkbeiner (2011). We assume that the extinction in the host

[1] http://sngroup.oapd.inaf.it

[2] http://www.pessto.org/pessto/index.py

[3] http://skyserver.sdss3.org/dr9/en/tools/chart/

galaxy is negligible, as we detect no sign of narrow interstellar Na I D absorption (Turatto, Benetti & Cappellaro 2003; Poznanski, Prochaska & Bloom 2012), even in spectra of higher S/N ratio (cf. Section 4).

From the narrow emission lines visible in the spectra with better S/N ratio (Hα, Hβ and [O III] 5007 Å lines; see Section 4), we derive a mean redshift $z = 0.2868 \pm 0.0006$, where the error is the standard deviation of several measurements. Assuming a Planck Universe ($H_0 = 67.3\,\mathrm{km\,s^{-1}\,Mpc^{-1}}$, $\Omega_\lambda = 0.685$ and $\Omega_\mathrm{m} = 0.315$ from Ade et al. 2013), the luminosity distance for CSS121015 is $d_\mathrm{l} = 1520$ Mpc and the distance modulus is $\mu = 40.91$ mag; these values are used throughout the paper.

Adopting the reddening and the distance modulus discussed above, we infer a magnitude of $M_r \gtrsim -17.9$ for the faint host galaxy of CSS121015.

3 OPTICAL PHOTOMETRY

Optical imaging data of CSS121015 were obtained using a number of different instrumental configurations. Basic information on these observations is reported in Tables 2 and 3. The measured position of the SN in several frames is RA = $00^\mathrm{h}\,42^\mathrm{m}\,44\overset{\mathrm{s}}{.}38 \pm 0\overset{\mathrm{s}}{.}03$; Dec. = $13^\circ\,28'\,26\overset{''}{.}197 \pm 0\overset{''}{.}05$.

The CCD frames were first bias and flat-field corrected in the usual manner. Since some of the data were obtained under non-photometric conditions, we measured relative photometry with respect to local field stars (see Fig. 1), whose magnitudes were computed by averaging estimates obtained on photometric nights.

Ideally, one would like to remove the galaxy background by subtraction of a galaxy 'template' (i.e. an image where the SN is absent). In the case of CSS121015, suitable template images were not available for the Johnson–Cousins frames. However, as the host galaxy is quite faint (see Section 2), the SN magnitudes could be safely measured via point spread function (PSF) fitting, provided we have decent seeing and the detector pixel scale allows for good PSF sampling. For the actual measurement, we used a dedicated, custom-built pipelines (developed by us, EC), consisting of a collection of PYTHON scripts calling standard IRAF tasks (through PYRAF), and specific data analysis tools, such as SEXTRACTOR (for source extraction and classification) and DAOPHOT (for PSF fitting). In our implementation of the PSF-fitting procedure, an initial estimate of the sky background at the SN location is obtained using a low-order polynomial fit to the surrounding region. This is subtracted from the image, before fitting the SN with a PSF model derived from isolated field stars. The fitted source is removed from the original image, an improved estimate of the local background is derived and the PSF-fitting procedure is iterated. The residuals are visually inspected to validate the fit.

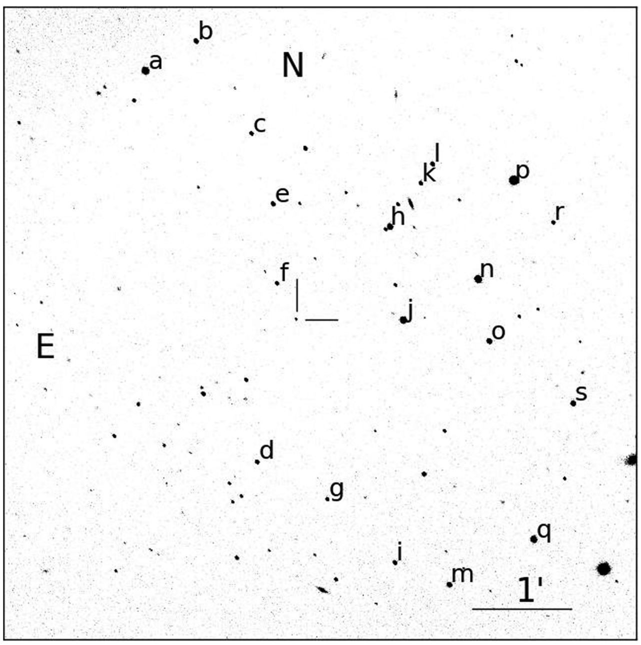

Figure 1. CSS121015 SN and reference stars. This is a TNG+LRS *R* frame taken on 2012 December 25. The measured seeing was 1.5 arcsec.

Error estimates were obtained through artificial star experiments, in which a fake star, of similar magnitude to the SN, is placed in the PSF-subtracted residual image in a position close to, but not coincident with, that of the real source. The simulated image is processed through the PSF-fitting procedure. This process is repeated at a number of positions; the dispersion of the magnitude returned by the pipeline is taken as an estimate of the instrumental magnitude error, accounting mainly for the background fitting uncertainty. This is combined (in quadrature) with the PSF-fit error returned by DAOPHOT, and the propagated errors from the photometric calibration.

3.1 Johnson–Cousins *UBVRI* photometry

Six photometric nights were used to calibrate the local stellar sequence, introduced in Section 3, against Landolt standard stars (Landolt 1992). The Johnson–Cousins magnitudes of the local standards, and their estimated errors, are shown in Table 1. In addition to standard *UBVRI* filters, CSS121015 was also observed with SDSS filters (cf. Section 3.2). In particular, we used the Liverpool Telescope (LT + RATCam) to get SDSS-*u*, Johnson-*BV* and SDSS-*ri*. These instrumental magnitudes were then transformed to Johnson-*UBV* and Cousins-*RI* magnitudes using colour equations, again derived through observations of Landolt fields, to enrich the *UBVRI* light curves. The final SN magnitudes (calibrated in the Vega system) are presented in Table 2. Sometimes the errors are relatively high, mostly because of poor sky transparency and/or poor seeing. The *UBVRI* light curves are plotted in Fig. 2.

Only the *V*-band light curve has pre-maximum points. They are from unfiltered (pseudo-*V*) CRTS observations. CRTS magnitudes have been obtained after template subtraction (see Section 3.2 for a description of this technique), with the template taken on 2012 June 22, well before the SN explosion. The magnitudes have been scaled to *V* using our local standards (see Table 1). The rising phase is steeper than the post-maximum decline. By fitting a low-order polynomial to the observed *V*-band light curve, we estimate that the maximum occurred on JD = 245 6226 ± 2, at $V = 18.34 \pm 0.10$ mag. Given the smooth rise shown by the *V* light curve, we fit a parabola to the flux derived from the first three points and estimate that the explosion occurred on JD = 245 6175 ± 10, e.g. about 10 d before discovery and 40 d before *V*-band maximum light (rest frame). The uncertainty in the explosion epoch accounts for the possibility of an early 'plateau'-like break, as seen in the rising light curve of one SLSN (see Leloudas et al. 2012). Although the explosion epoch would allow the most physically meaningful comparisons with other SNe, its large associated error means that we prefer to use the time of maximum light as a reference epoch.

The post-maximum declines are approximately linear in all bands, and the light curves never show a break in their decline. The observed declines are progressively slower as we move from

Table 1. Magnitudes of local sequence stars identified in Fig. 1.

Star	RA	Dec.	*U*	err*U*	*B*	err*B*	*V*	err*V*	*R*	err*R*	*I*	err*I*
a	0:42:52.689	13:31:46.32	15.72	0.04	15.73	0.01	15.03	0.01	14.65	0.01	14.25	0.01
b	0:42:49.903	13:32:10.22	17.87	0.02	18.06	0.02	17.32	0.01	16.95	0.01	16.52	0.04
c	0:42:46.848	13:30:55.87			19.09	0.02	18.11	0.01	17.56	0.01	17.01	0.04
d	0:42:46.531	13:26:31.35			19.28	0.01	17.95	0.01	17.18	0.01	16.50	0.01
e	0:42:45.662	13:29:59.14			19.80	0.01	18.12	0.01	17.12	0.01	16.01	0.02
f	0:42:45.450	13:28:55.00			20.44	0.05	18.87	0.01	17.87	0.01	16.64	0.01
g	0:42:42.641	13:26:01.14	19.10	0.08	19.30	0.02	18.53	0.01	18.14	0.01	17.70	0.02
h	0:42:39.203	13:29:40.90			17.01	0.01	16.15	0.01				
i	0:42:38.896	13:25:09.59	17.93	0.01	18.67	0.02	17.84	0.01	17.40	0.01	16.95	0.03
j	0:42:38.450	13:28:25.51	16.27	0.02	16.11	0.01	15.31	0.01	14.89	0.01	14.50	0.02
k	0:42:37.487	13:30:15.87	18.80	0.05	18.78	0.01	17.90	0.01	17.46	0.01	16.94	0.02
l	0:42:36.836	13:30:31.45			18.53	0.02	17.53	0.01	17.01	0.01	16.48	0.03
m	0:42:35.875	13:24:51.53	17.16	0.04	17.45	0.02	16.82	0.01	16.43	0.01	15.95	0.02
n	0:42:34.314	13:28:58.59	16.90	0.01	16.09	0.01	15.05	0.01	14.48	0.01	13.98	0.01
o	0:42:33.686	13:28:08.43	17.47	0.01	17.39	0.01	16.62	0.01	16.21	0.01	15.74	0.02
p	0:42:32.321	13:30:18.29	15.56	0.01	15.10	0.01	14.14	0.01	13.65	0.01		
q	0:42:31.195	13:25:28.07	17.14	0.05	16.66	0.01	15.70	0.01	15.20	0.01		
r	0:42:30.116	13:29:44.29			19.53	0.02	18.48	0.01	17.89	0.01	17.26	0.02
s	0:42:29.068	13:27:18.36	17.71	0.03	17.69	0.01	16.80	0.01			15.78	0.01

Table 2. Johnson–Cousins photometric measurements for CSS121015, calibrated in the Vega system.

Date	JD (−240 0000)	Phase[a] (d)	*U*	err*U*	*B*	err*B*	*V*	err*V*	*R*	err*R*	*I*	err*I*	Instrument
2012-09-16	561 86.74	−39(−30)					20.95	0.56					CRTS
2012-09-25	561 95.87	−30(−23)					19.76	0.28					CRTS
2012-10-06	562 06.72	−19(−15)					18.82	0.20					CRTS
2012-10-15	562 15.74	−10(−8)					18.55	0.35					CRTS
2012-10-19	562 19.92	−6(−5)			18.53	0.03	18.42	0.02	18.22	0.02			AF
2012-10-21	562 21.92	−4(−3)					18.38	0.29					CRTS
2012-10-22	562 22.83	−3(−2)	17.83	0.04	18.54	0.02	18.35	0.03	18.24	0.02	18.13	0.02	AF
2012-10-26	562 26.11	0(0)			18.29	0.20	18.19	0.10	18.20	0.06	18.00	0.07	RAT
2012-11-05	562 36.99	+11(+9)	18.17	0.04	18.70	0.02	18.52	0.02	18.33	0.02	17.91	0.02	AF
2012-11-06	562 38.10	+12(+9)	18.39	0.08	18.99	0.02	18.67	0.02	18.37	0.18	18.26	0.04	EF2
2012-11-07	562 38.80	+13(+10)	18.23	0.03	18.85	0.02	18.45	0.02	18.30	0.02	18.25	0.02	AF
2012-11-12	562 43.64	+18(+14)					18.72	0.27					CRTS
2012-11-12	562 44.10	+18(+14)	18.64	0.09	19.10	0.07	18.73	0.05	18.49	0.12	18.19	0.07	EF2
2012-11-18	562 49.05	+23(+18)	18.62	0.02	19.22	0.02	18.72	0.02	18.47	0.02	18.15	0.02	LRS
2012-11-20	562 51.59	+26(+20)					18.96	0.21					CRTS
2012-11-23	562 54.13	+28(+22)	19.17	0.09	19.52	0.04	18.98	0.02	18.75	0.02	18.34	0.03	EF2
2012-11-30	562 61.84[b]	+36(+28)	19.76	0.17	19.81	0.06	19.07	0.02	18.76	0.02	18.27	0.02	RAT
2012-12-04	562 65.84	+40(+31)	19.77	0.17	19.98	0.06	19.16	0.06	18.90	0.04	18.43	0.02	RAT
2012-12-05	562 66.74	+41(+31)					19.34	0.22					CRTS
2012-12-05	562 66.85	+41(+32)	19.85	0.16	19.92	0.04	19.22	0.03	18.81	0.02	18.39	0.02	RAT
2012-12-05	562 67.00	+41(+32)	19.90	0.09	20.03	0.04	19.32	0.05	18.96	0.04	18.46	0.04	EF2
2012-12-06	562 67.76	+42(+33)	19.75	0.22	20.11	0.13	19.28	0.06	18.89	0.03	18.58	0.05	AF
2012-12-07	562 68.85	+43(+33)			20.23	0.04	19.23	0.04	18.96	0.03	18.40	0.03	RAT
2012-12-09	562 70.85	+45(+35)			20.24	0.06	19.34	0.03	19.05	0.02	18.44	0.02	RAT
2012-12-12	562 74.10	+48(+37)	20.31	0.10	20.43	0.04	19.57	0.02	19.13	0.15	18.61	0.05	EF2
2012-12-15	562 76.84	+51(+40)			20.55	0.11	19.56	0.04	19.06	0.03	18.53	0.03	RAT
2012-12-17	562 78.81	+53(+41)					19.74	0.04	19.17	0.04			AF
2012-12-18	562 79.87	+54(+42)			20.67	0.10	19.58	0.03	19.14	0.02	18.68	0.02	RAT
2012-12-18	562 79.88	+54(+42)			20.68	0.13							AF
2012-12-22	562 84.00	+58(+45)	20.64	0.10	20.96	0.11	19.85	0.03	19.26	0.03	18.72	0.02	LRS
2012-12-25	562 86.75	+61(+47)	20.68	0.09	20.97	0.05	19.94	0.03	19.40	0.02	18.93	0.02	LRS
2012-12-27	562 88.85	+63(+49)			20.99	0.14	19.95	0.11	19.47	0.05	18.76	0.02	RAT
2013-01-02	562 95.10	+69(+54)			21.43	0.04	20.26	0.03	19.64	0.03	18.91	0.05	EF2
2013-01-08	563 00.75	+75(+58)	21.65	0.06	21.60	0.02	20.50	0.02	19.69	0.02	19.00	0.02	LRS
2013-01-12	563 04.83	+79(+61)			21.90	0.06	20.56	0.05	19.86	0.03	19.10	0.06	RAT
2013-01-15	563 07.88	+82(+64)			22.12	0.10	20.65	0.18	20.05	0.07	19.20	0.03	RAT
2013-01-24	563 16.87	+91(+71)			22.24	0.26	21.02	0.15	20.25	0.06	19.43	0.02	RAT

Table 2 – *continued*

Date	JD (−240 0000)	Phase[a] (d)	U	errU	B	errB	V	errV	R	errR	I	errI	Instrument
2013-01-27	563 20.00	+94(+73)					21.27	0.11	20.18	0.07	19.56	0.17	LRS
2013-01-28	563 20.84	+95(+74)			22.58	0.18	21.08	0.13	20.29	0.06	19.54	0.04	RAT
2013-01-30	563 22.74	+97(+75)					21.21	0.14	20.37	0.06	19.71	0.08	AF

[a]Relative to the estimated epoch of the *V* maximum (JD = 245 6226); the phase in parenthesis is in the SN rest frame. The rise to maximum *V* lasted ∼51 d (∼40 d in the rest frame).
CRTS = Catalina Real-time Transient Survey
AF = Asiago 1.82 m Telescope + AFOSC
RAT = Liverpool Telescope + RATCam (SDSS *u*, *r*, *i* and Johnson *B*, *V*)
EF2 = ESO-NTT + EFOSC2
LRS = TNG + LRS
[b]For JD = 245 6264.72, we have also NIR LBT–LBT utility camera (& spectrograph) imaging fields for extragalactic research (LUCIFER) observations (on 2MASS scale): $J = 18.46 \pm 0.05$; $H = 18.34 \pm 0.04$; $K = 17.94 \pm 0.06$.

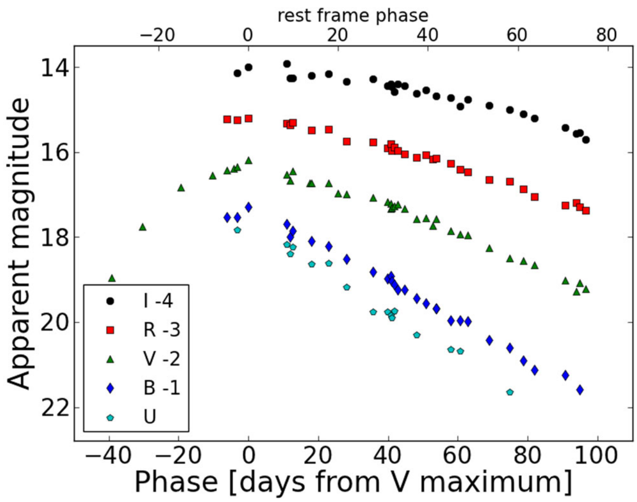

Figure 2. Johnson–Cousins *U* (top), *B*, *V*, *R* and *I* (bottom) light curves of CSS121015. The phase given is in the observer frame (bottom *x*-axis) and SN rest frame (top *x*-axis).

the *U* to the *I* band. Starting from maximum light, the observed linear decline rates are 5.40 ± 0.20, 4.53 ± 0.10, 3.23 ± 0.08, 2.43 ± 0.08 and 1.92 ± 0.11 mag $(100\,\mathrm{d})^{-1}$ in *U*, *B*, *V*, *R* and *I*, respectively.

3.2 SDSS *griz* photometry

CSS121015 was observed in the SDSS *griz* bands with the Faulkes North Telescope, equipped with the MEROPE1 and Spectral2 cameras. Table 3 integrates these data with the *ri* data from LT+RATCam, mentioned above, collecting all SDSS photometry. This was reduced with the same recipes used for the Johnson–Cousins photometry. The photometric calibration was achieved by comparing the magnitudes obtained for the stars in the field of CSS121015 with their SDSS magnitudes, and is therefore close to the AB system ($g, r, i_{\mathrm{SDSS}} \sim g, r, i_{\mathrm{AB}}$, while $z_{\mathrm{SDSS}} \sim z_{\mathrm{AB}} - 0.02$ mag;[4] all magnitudes given in Table 3 are in the ABmag system.).

In the table, we also report deep *r* and *i* limits obtained with WHT+ACAM and TNG+LRS at about 200 d (rest frame) after maximum. These will turn out to be very important in deriving an upper limit to the ^{56}Ni mass synthesized in the explosion (see Section 6).

Given the low surface brightness of the host galaxy, we were able to obtain reliable deep limits directly on the *r* and *i* images. However, we checked these with template subtraction. This technique requires that exposures of the field, obtained before the explosion or long after the SN has faded, are available. The templates have been taken with the same filters used for SN imaging, with high S/N ratio and good seeing. While in principle they should be obtained with the same telescopes as those used for the specific SN observations (to guarantee the same bandpass), in practice archival images with the proper filters in the online archives are very welcome. In our case, we were able to retrieve deep pre-discovery exposures in the *r*, *i* bands from SDSS3-DR9.

In template subtraction, the template image is first geometrically registered to the same pixel grid as the SN frame. The PSF of the two images is then matched by means of a convolution kernel determined by comparing a number of reference sources in the field (for this we used HOTPANTS[5]). After matching the photometric scale, the template image is subtracted from the SN image, and a difference image is obtained. In our case, no residuals were detectable in the *r*- and *i*-band frames at the SN location, so we can only estimate an upper limit to the SN magnitude.

The limits were estimated through artificial star experiments, in which a fake star of a given magnitude is placed in the original frame at the precise position of the source. The process is iterated several times by injecting fainter and fainter fake stars. The limit is given by the magnitude of the fake star that leaves detectable residuals after template subtraction. As already stated, the limits obtained with template subtraction agree well with those derived directly on the deep observed images (given in Table 3).

4 SPECTROSCOPY

Our spectroscopic observations cover a time interval from day −6 to day +85 (in the observer frame) from the estimated maximum epoch. Table 4 lists the date (column 1), the JD (column 2), the observed (and rest-frame) phases relative to the explosion (column 3), the wavelength range (column 4), instrument used (column 5) and the resolution as measured with a Gaussian fit of the night-sky lines (column 6). For some epochs, we co-added near-contemporaneous spectra to improve the S/N.

The spectra were reduced using standard IRAF routines. Extractions were variance-weighted, based on the data values and a Poisson/CCD model using the gain and readout noise parameters.

[4] http://www.sdss3.org/dr9/algorithms/fluxcal.php#SDSStoAB

[5] http://www.astro.washington.edu/users/becker/hotpants.html

Table 3. SDSS Photometry in *griz* bands, calibrated in the ABmag system.

Date	JD (−240 0000)	Phase[a] (d)	g	err$g$	r	err$r$	i	err$i$	z	err$z$	Instrument[b]
2012-10-26	562 26.10	0(0)			18.42	0.12	18.25	0.18			RAT
2012-10-30	562 31.00	+5(+4)	18.50	0.30	18.42	0.16					Fau2
2012-11-02	562 33.90	+8(+6)	18.51	0.04	18.49	0.02	18.62	0.07	18.56	0.06	Fau2
2012-11-05	562 36.70	+11(+9)	18.62	0.04	18.52	0.02	18.58	0.07	18.59	0.04	Fau2
2012-11-09	562 40.70	+15(+12)	18.69	0.06	18.57	0.02	18.65	0.07	18.55	0.04	Fau2
2012-11-11	562 42.70	+17(+13)	18.83	0.05	18.63	0.04	18.67	0.09	18.56	0.08	Fau2
2011-11-15	562 46.80	+21(+16)	18.84	0.07	18.73	0.04	18.75	0.08			Fau2
2012-11-26	562 57.80	+32(+25)	19.18	0.09	18.78	0.13	18.76	0.10	18.83	0.10	Fau1
2012-11-30	562 61.84	+36(+28)			18.97	0.04	18.75	0.03			RAT
2012-12-02	562 63.70	+38(+30)	19.51	0.06	19.02	0.04	18.94	0.07	18.67	0.10	Fau1
2012-12-04	562 65.83	+40(+31)			19.10	0.03	18.91	0.03			RAT
2012-12-05	562 66.84	+41(+32)			19.04	0.03	18.85	0.03			RAT
2012-12-07	562 68.84	+43(+33)			19.21	0.04	18.91	0.06			RAT
2012-12-09	562 70.84	+45(+35)			19.29	0.03	18.96	0.03			RAT
2012-12-14	562 75.80	+50(+39)	19.96	0.08	19.31	0.08	19.03	0.09			Fau1
2012-12-15	562 76.83	+51(+40)			19.34	0.04	19.00	0.05			RAT
2012-12-18	562 79.86	+54(+42)			19.39	0.03	19.11	0.03			RAT
2012-12-27	562 88.84	+63(+49)			19.74	0.05	19.29	0.03			RAT
2013-01-12	563 04.82	+79(+61)			20.19	0.05	19.67	0.12			RAT
2013-01-15	563 07.87	+82(+64)			20.34	0.06	19.90	0.08			RAT
2013-01-24	563 16.86	+91(+71)			20.61	0.07	20.00	0.04			RAT
2013-01-28	563 20.83	+95(+74)			20.65	0.07	20.10	0.09			RAT
2013-06-10	564 53.75	+228(+177)			>22.4	0.2					ACA
2013-06-11	564 54.67	+229(+178)					>22.4	0.2			ACA
2013-07-15	564 88.69	+263(+204)			>23.1	0.3					LRS

[a]Relative to the estimated epoch of V maximum light (JD = 245 6226); the phase in parenthesis is in the SN rest frame.
[b]See note to Table 2 for instrument coding, plus:
Fau1 = Faulkes Telescope North+EM01
Fau2 = Faulkes Telescope North+fs02
ACA = WHT + ACAM

The background at either side of the SN signal was fitted with a low-order polynomial and then subtracted. Fluxing and telluric absorption modelling were achieved using observations of spectrophotometric standard stars. For ESO faint object spectrograph and camera (EFOSC) spectra, all the previous steps were optimized in a custom-built PYTHON/PYRAF package (PESSTO-NTT pipeline) developed by one of us (SV) including also an automatic check of the wavelength calibration using the sky lines. Most spectra have been taken with the slit aligned along the parallactic angle. The flux calibration of the spectra was checked against the photometry (using the IRAF task *stsdas.hst_calib.synphot.calphot*) and, when discrepancies occurred, the spectral fluxes were scaled to match the photometry. On nights with fair to good sky conditions, the agreement with photometry was within 15 per cent. A selection of the CSS121015 spectra is shown in Fig. 3.

The last EFOSC2 spectra, taken about one year after the SN explosion (rest frame) when the SN had faded away, are that of the host galaxy. To increase the S/N, we co-added the six spectra for a total exposure time of 16 200 s. In order to put the faint host galaxy in the slit, we used star f (see Fig. 1) as guide and rotated the slit to a position angle of 28°.3. The photometry synthesized from the spectra of star f (in comparison with the magnitudes given in Table 1) was used to normalize the flux of the galaxy spectra. While the host galaxy spectra were obtained under low-to-average sky conditions, after computing a weighed mean of the six individual spectra, according to the S/N, the resulting combined spectrum (see boxes a and b of Fig. 3) was good enough for our purposes (see Section 4.1).

4.1 Spectroscopic evolution and comparison with other SLSNe-II

The early spectra show a very blue continuum ($T_{\rm BB} \sim 17\,700$ K, after reddening and redshift corrections). This becomes progressively redder with phase, reaching a temperature of about 5500 K at +85 d. Initially, the spectra are almost featureless, with the first broad features – mostly due to Fe II lines – becoming visible in the spectrum at +21 d. The spectrum at −3/−2 d (see Figs 3 and 4) shows a narrow, barely resolved Hα emission, and no clear broad Balmer features.

However, the high-S/N-ratio spectra at phases +58/+61 d show a dim and broad (FWHM $\sim$ 10 000 km s^{-1}) Hα emission, with the faint, narrow component superimposed (and only marginally resolved on top of it). In the blue part of the spectrum, narrow Balmer and [O III] emission lines are also visible. From the narrow Balmer lines of the +85 d spectrum, we derive a Gaussian full width at half-maximum (FWHM) $\lesssim$ 600 km s^{-1}. Whether the narrow lines are intrinsic to the SN or are of interstellar origin is difficult to establish, mostly because of the relatively low S/N ratio of the first spectra, although the upper limit of 600 km s^{-1} of the narrow Balmer lines is consistent with fast wind of massive stars. Moreover, the luminosities of the narrow hydrogen (Hα, Hβ and Hγ) and O III 5007 Å line show a smooth decrease (see Fig. 5), suggesting that the narrow H and [O III] 5007 Å lines are related to the SN event. To settle this issue, we analysed the host galaxy spectrum taken almost a year after the SN went off. Given the faintness of the host, the spectrum is relatively noisy, but it shows a weak continuum

Table 4. Spectroscopic observations of CSS121015.

Date	JD (−240 0000)	Phase[a] (d)	Range (Å)	Instrument[b]	Resolution (Å)
2012-10-19	562 20.38	−6(−4)	3500–8200	AF	13.5
2012-10-22	562 23.29	−3(−2)	3500–8200	AF	13.5
2012-10-22	562 23.62	−2(−1.5)	3200–9000	ISI	6
2012-11-05	562 37.38	+11(+9)	3500–8200	AF	13.5
2012-11-07	562 38.65	+13(+10)	3650–9300	EF2	18
2012-11-07	562 39.33	+13(+10)	3500–8200	AF	13.5
2012-11-13	562 44.58	+19(+15)	3650–9300	EF2	18
2012-11-15	562 46.56	+21(+16)	3650–9300	EF2	18
2012-11-18	562 49.50	+24(+19)	3200–8000	LRS	10.5
2012-11-20	562 52.47	+26(+20)	3500–9800	ISI	7
2012-11-23	562 54.59	+29(+23)	3650–9300	EF2	18
2012-12-03	562 64.76	+39(+30)	9500–13500	Luc	3
2012-12-04	562 66.30	+40(+31)	3500–8200	AF	13.5
2012-12-06	562 67.56	+42(+33)	3650–9300	EF2	18
2012-12-09	562 71.29	+45(+35)	3500–8200	AF	13.5
2012-12-13	562 74.55	+49(+38)	3650–9300	EF2	18
2012-12-14	562 76.46	+50(+39)	3200–10 000	LRS	10.5
2012-12-22	562 84.38	+58(+45)	3200–10 000	LRS	10.5
2012-12-25	562 87.36	+61(+47)	3200–10 000	LRS	10.5
2013-01-18	563 11.33	+85(+66)	3600–10 000	OSI	9
2013-11-26	566 22.61	+397(+309)	3650–9250	EF2	28
2013-12-02	566 28.54	+403(+313)	4800–9250	EF2	28
2013-12-03	566 29.55	+404(+314)	4800–9250	EF2	28
2013-12-25	566 51.56	+426(+331)	4800–9250	EF2	28
2013-12-26	566 52.59	+427(+332)	4800–9250	EF2	28
2013-12-27	566 53.56	+428(+333)	4800–9250	EF2	28

[a]Relative to the estimated epoch of the V maximum (JD = 245 6226); the phase in parenthesis is in the SN rest frame. [b]See note to Table 2 for instrument coding, plus:
ISI = WHT+ISIS
Luc = LBT+LUCIFER (flat continuum, noisy spectrum)
OSI = GTC+OSIRIS

from which a synthetic r magnitude of 22.7 ± 0.5 was derived, that is consistent with the magnitude derived from deep imaging (see Table 3) of $r \sim 23.0$. There is no sign of narrow emission line in the co-added spectrum (see Figs 3–5), and we derive the following upper limits: $F(\mathrm{H}\gamma) \leq 7.0 \times 10^{-17}$ erg s^{-1} cm^{-2}, $F(\mathrm{H}\beta) \leq 1.0 \times 10^{-17}$ erg s^{-1} cm^{-2}, F([O III] 5007 Å]) $\leq 3.5 \times 10^{-17}$ erg s^{-1} cm^{-2} and $F(\mathrm{H}\alpha) \leq 4.9 \times 10^{-17}$ erg s^{-1} cm^{-2}.

These upper limits prove that the narrow lines seen in the early spectra are indeed intrinsic to the SN event and that CSM was surrounding the SN ejecta. Interestingly, flux variation of [O III] and Balmer lines has previously been detected in SNe IIn (e.g. in Turatto et al. 1993).

Given the clear presence of a broad Hα line in the spectra later than +49/+50 d and of narrow lines along its spectral evolution, we may finally classify CSS121015 as a Type II/IIn SN.

At this time, the blue part of the spectrum is dominated by broad metal features, mostly belonging to the Fe group, with some contribution from Ca II H&K and Mg II. The spectra show little evolution between 50 d and the end of our observations, and never show any hint of O, though we detect what may be a weak [Ca II] 7300 Å line. As shown in Fig. 4 and in the inset of Fig. 3, the Hα emission shows a slightly asymmetric, triangular profile, with a red wing extending up to $v_{ZI} \sim 10\,000$ km s^{-1}.

In Fig. 6, the CSS121015 spectra are compared with other very luminous SNe at similar phases. The comparison SN sample (SNe 2005gj, 2008es and 2008fz) has been selected using the GELATO comparison tool[6] (Harutyunyan et al. 2008) as the objects that give the best overall match to CSS121015 in particular at late times, when the SN features became stronger. Up to day ∼+20 (rest frame), the spectra are dominated by a blue continuum, and only the +18 d SN 2005gj spectrum shows broad features, at this time. In the ejecta–CSM interaction scenario, this can be attributed to the CSM shell in SN 2005gj having a smaller radius (fainter luminosity, see Fig. 7) and lower density than the CSM around the other SNe, therefore revealing the underlying SN earlier. The broad bump at ∼4600 Å, visible in the +19/20 d CSS121015 spectrum, is also detected in SN 2008es at a similar phase, while the SN 2008fz spectrum at a slightly later phase (+49 d) shows stronger features. At +38/39 d, the spectra of the four SNe are extraordinarily similar, with the exception of the narrower Hα components, which are stronger in SN 2005gj. This SN shows prominent intermediate and narrow line profiles, which suggests the presence of a more extended, dilute, and H-rich CSM. The broad components have similar profiles, with terminal velocities of $\sim 10\,000$ km s^{-1}. The spectra at late phases also show very good agreement, and are all dominated in the blue by transitions of iron group elements. The spectral energy distributions (SEDs) of the SNe in our sample are very similar at all epochs.

[6] https://gelato.tng.iac.es; the list of GELATO templates is given here: https://gelato.tng.iac.es/templates

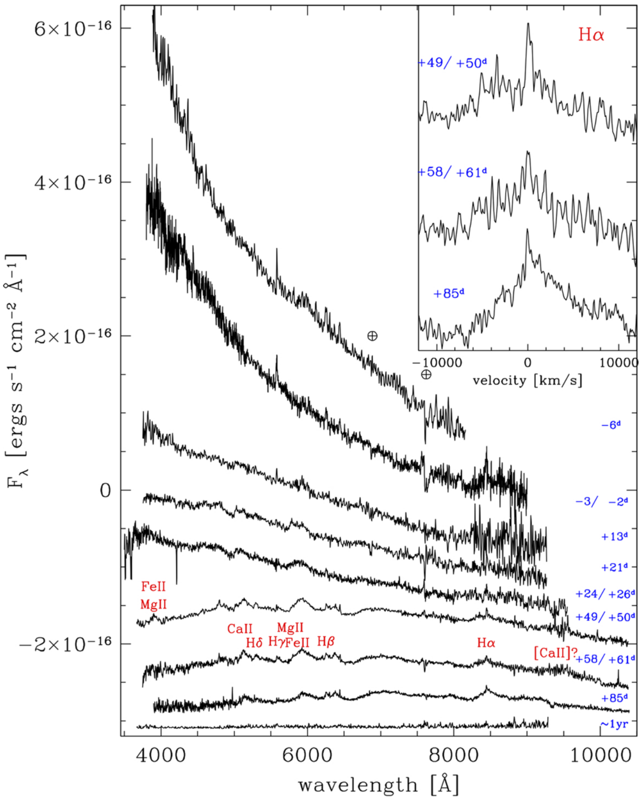

Figure 3. Spectral evolution of CSS121015. Wavelength and phases (from maximum) are in the observer's frame. The ordinate refers to the first spectrum, and the others have been arbitrarily shifted downwards. The −3/−2 d spectrum is a merge of the AFOSC and ISIS spectra. The +13 d spectrum is the average of the AFOSC and EFOSC2 spectra. The +24/+26 d spectrum is a merge of the LRS and ISIS spectra. The +49/+50 d spectrum is the average of the EFOSC2 and LRS spectra. Finally, the +58/61 d spectrum is the average of two LRS spectra (see Table 4). The last spectrum is the host galaxy spectrum taken about 400 d after maximum. Residuals from the atmospheric absorption corrections have been marked with the ⊕ symbol. The inset shows the evolution of the Hα profile, in velocity space.

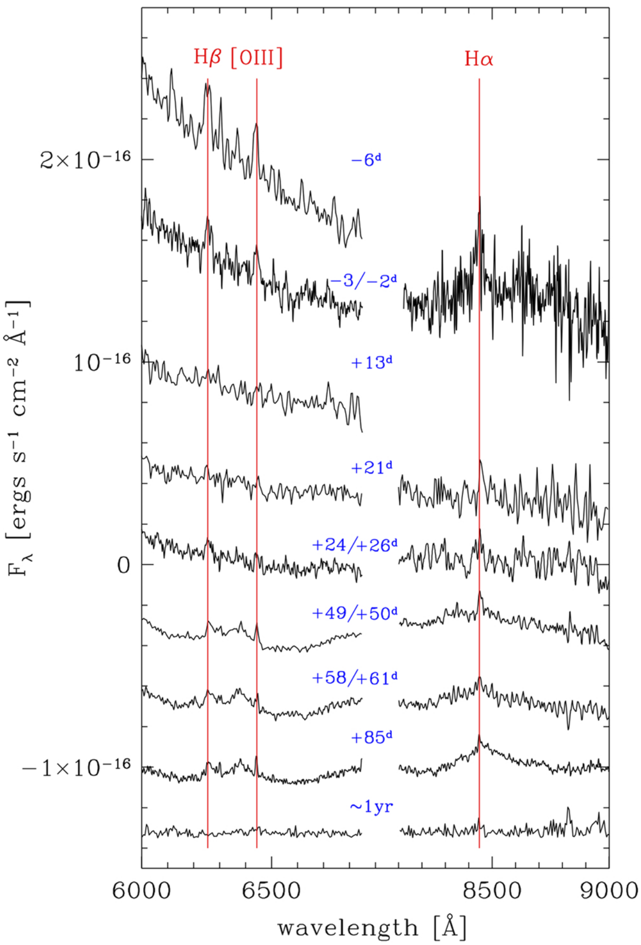

Figure 4. Spectral evolution of CSS121015 zoomed on the narrow Hβ, [O III] 5007 Å and Hα transitions. Wavelength and phases are as in Fig. 3.

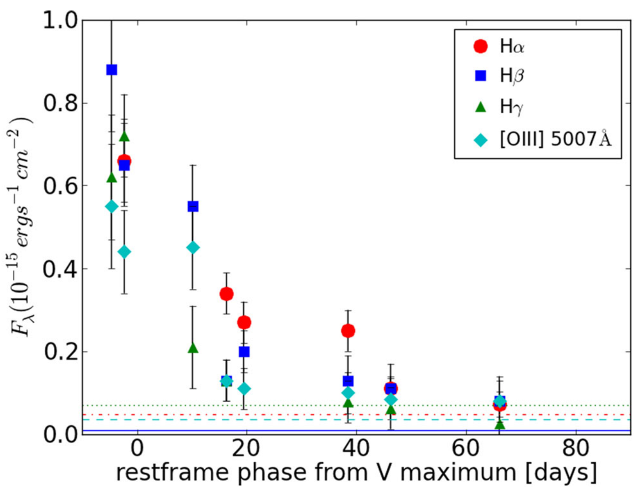

Figure 5. Flux evolution of the narrow Balmer and [O III] 5007 Å lines. The reported flux is the true flux of the lines above the continuum. The lines mark the values of the upper limits derived for the four emission lines in the host spectrum taken on 2013 November–December (see Table 4; dash–dotted, red, line refers to Hα emission; solid, blue, line to Hβ; dotted, green, line to Hγ; and dashed, cyan, line to [O III] 5007 Å). The last deep spectra of the host galaxy show that the contamination of the narrow line emissions from the host is negligible.

5 BOLOMETRIC LIGHT CURVE

The pseudo-bolometric light curve of CSS121015 has been computed by integrating its multicolour photometry from U to z, neglecting any possible contribution in the low- (infrared/radio) and high-energy (UV, X-ray) domains. We proceeded by deriving, for each epoch and filter, the flux at the effective wavelength. We adopted as reference the epochs of the V-band photometry, and missing measurements at given epochs for the other filters were obtained through interpolation or, if necessary, by extrapolation assuming a constant colour from the closest available epoch. The fluxes at the filter effective wavelengths, corrected for extinction, provide the SED at each epoch, which is integrated by the trapezoidal rule, assuming zero flux at the integration boundaries. The observed flux was converted into luminosity for the adopted distance.

The pseudo-bolometric light curve is shown in Figs 8 and 9.

Given the high temperature, the wavelength ranges of our optical spectra only sample the Rayleigh–Jeans tail of the CSS121015 SED. This means that the temperatures derived from the early spectra have significant errors (up to ∼10 per cent). This also implies that there is significant emission outside the observed spectral range.

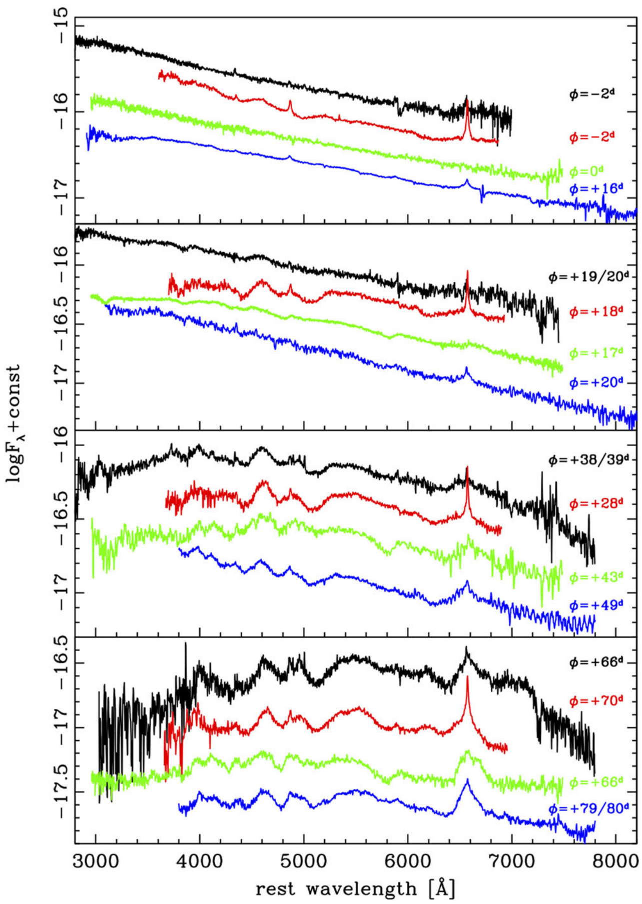

Figure 6. Comparison of the spectra of CSS121015 with those of a selected sample of luminous SNe at significant epochs (cf. Section 4.1). From top to bottom in each panel: spectra of CSS121015 (black), SN 2005gj (Aldering et al. 2006; Prieto et al. 2007, red), SN 2008es (Gezari et al. 2009; Miller et al. 2009, green) and SN 2008fz (Agnoletto 2010, blue). The spectra have been corrected for redshift and reddening. The rest-frame phases are from the estimated dates of maximum.

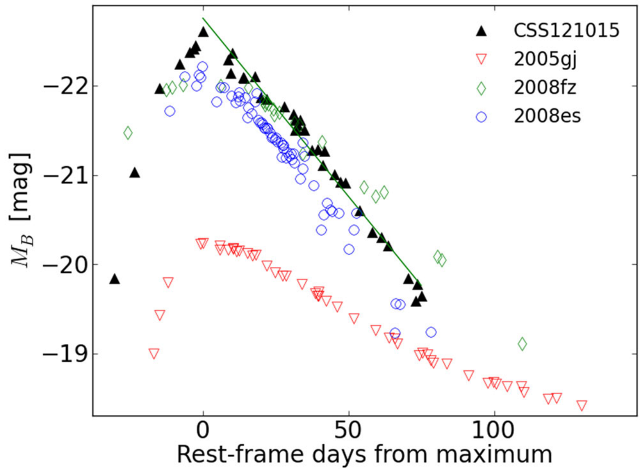

Figure 7. Comparison of the absolute *B*-band light curve of CSS121015 with those of SNe 2005gj, 2008es and 2008fz. The phases have been corrected for the time dilation due to cosmic expansion; a *K*-correction has been applied, following the Kim et al. (1996) recipe. SN 2005gj is the nearest SN (z = 0.06 and photometry from Aldering et al. 2006; Prieto et al. 2007). We have adopted only Galactic absorption correction (from $E(B-V) = 0.107$ mag; Schlafly & Finkbeiner 2011) and maximum epoch JD = 245 3658 (Prieto et al. 2007). SN 2008es is at a distance similar to that of CSS121015 (z = 0.202 taken from the Asiago Supernova Catalogue, ASC). The photometry and maximum epoch (JD = 245 4603) are from Gezari et al. (2009) and Galactic reddening ($E(B-V) = 0.010$ mag) from Schlafly & Finkbeiner (2011). For SN 2008fz (redshift $z = 0.133$, from ASC), the photometry and maximum epoch (JD = 245 4731) are from Drake et al. (2010), Agnoletto (2010) and Benetti et al. (in preparation). A correction for Galactic reddening of $E(B-V) = 0.036$ mag (Schlafly & Finkbeiner 2011) has been applied. The linear fit of CSS121015 past maximum points is shown with a solid (green) line.

If we assume that the SED can be well fitted with a blackbody (BB), and we calculate the flux below it, the extrapolated flux that may be regarded as an upper limit to the real flux emitted by CSS121015 in that particular phase, because in real SNe the UV region of the spectra can be affected by severe line blanketing, which shifts the emitted flux to longer wavelengths. This is why the integrated BB emission is giving us only an upper limit to the real SED. We see evidence for this line blanketing in the later, cooler spectra, with SED maxima well inside the observed wavelength range. The true luminosity falls somewhere between the pseudo-bolometric luminosity and the BB extrapolation. Approximating the SN as a BB also allows us to estimate a radius of the emitting region.

The BB extrapolated light curve is shown in Fig. 8. The CSS121015 bolometric light curve shows a relatively fast rise to maximum of about 40 d, and a slower post-maximum linear decline up to phase of about 80 d past maximum in the rest frame. It reaches a very bright peak of about $\log L = 44.50$ dex (∼44.9 in the BB extrapolation, see Table 5). The late deep *r*, *i* photometric limits (see Table 3) translate into an upper limit of $\log L = 42.40$ dex.

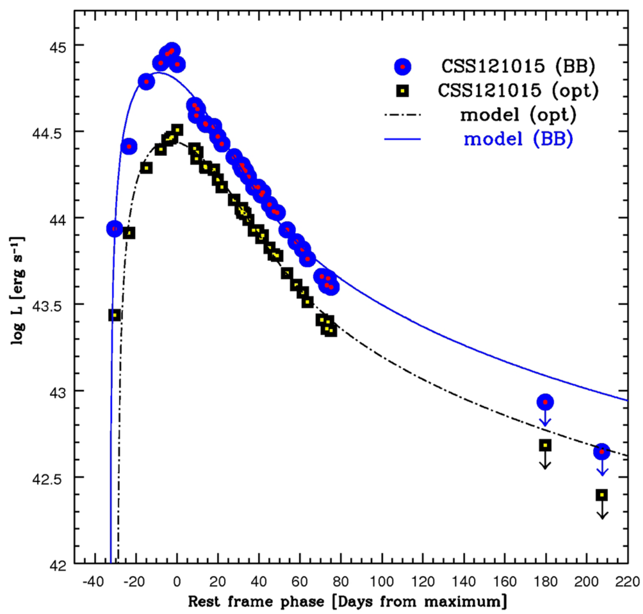

Figure 8. Comparison among the pseudo-bolometric light curve of CSS121015 obtained integrating the optical contribution only, the BB bolometric curve of CSS121015 and the two magnetar models described in the text that well reproduce the two curves.

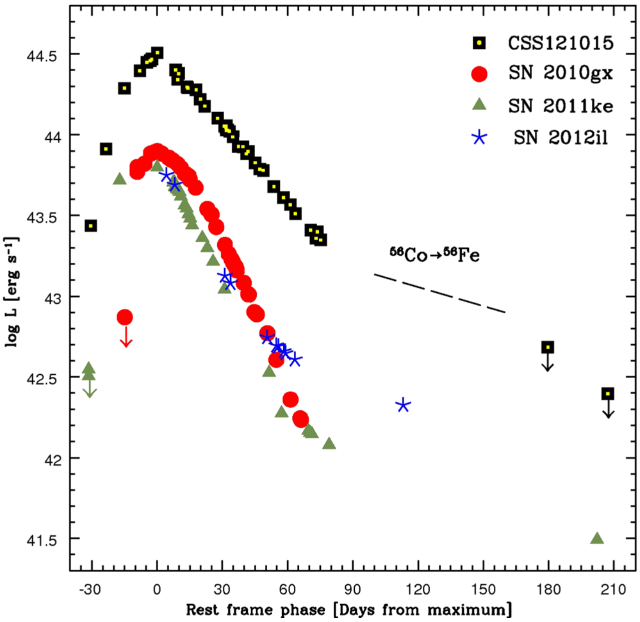

Figure 9. Comparison of the quasi-bolometric light curves of CSS121015 and the SLSNe-Ic 2010gx ($z \sim 0.23$, $E(B-V) = 0.04$ mag from Pastorello et al. 2010b), 2011ke ($z \sim 0.143$, $E(B-V) = 0.01$ mag from Inserra et al. 2013) and 2012il ($z \sim 0.175$, $E(B-V) = 0.02$ mag from Inserra et al. 2013). The curves have been corrected for time dilation.

Table 5. Radii deduced for CSS121015.

Phase[a] (d)	$\log L^b_{UBVRIz}$	T (K)	$\log L^b_{BB}$	R_{UBVRIz} (au)	R_{BB} (au)
−4	44.45	17 700	44.93	134	232
−2	44.47	17 300	44.93	144	245
+10	44.45	11 700	44.71	283	391
+14	44.24	10 300	44.50	311	421
+39	43.93	8400	44.15	327	424
+47	43.79	6700	44.04	438	586
+66	43.44	5500	43.82	434	672

[a]Rest-frame phase relative to the estimated epoch of the V maximum (JD = 245 6226).
[b]The steps followed for the computation of L_{UBVRiz} and L_{BB} are described in Section 5.

6 DISCUSSION

6.1 Absolute magnitudes of CSS121015 and comparison with other SLSNe

Taking into account the redshift, the observed V light curve shown in Section 3.1 has been translated, after K-correction (Kim, Goobar & Perlmutter 1996), to a B light curve in the host galaxy rest frame (see Fig. 7). With the adopted distance modulus and extinction, the absolute magnitude at maximum is $M_B = -22.6 \pm 0.1$ for CSS121015, which makes it one of the most luminous SNe ever observed. Moreover, the post-maximum rest-frame B decline is almost linear (see Fig. 7), with a rest-frame decay rate of ∼4.0 mag $(100\,\mathrm{d})^{-1}$, typical of Type II-Linear SNe (Patat et al. 1994), or a rapidly declining SN following Arcavi et al. (2012).

Fig. 7 shows a comparison of the B-band light curve of CSS121015 with the other superluminous, hydrogen-rich transients, namely SN 2008es (Gezari et al. 2009) and SN 2008fz (Agnoletto 2010; Drake et al. 2010, Benetti et al., in preparation). We also show the Type IIn SN 2005gj that is spectroscopically very similar to the other SNe of the sample. We stress that SN 2005gj has been explained in terms of an interacting SN Ia (Aldering et al. 2006; Prieto et al. 2007). However, this interpretation has been questioned by Benetti et al. (2006), Trundle et al. (2008) and Inserra et al. (2014) for this class of objects, since a scenario involving the interaction between an energetic SN Ic and a dense CSM could also explain the observations.

The shape of the M_B light curve of CSS121015 is very similar to that of SN 2008es, whose rising branch is, in this band, less constrained. However, the Robotic Optical Transient Search Experiment (ROTSE) unfiltered light curve indicates that the rising of SN 2008es is much steeper than that of CSS121015. Instead, the SN 2008fz light curve is slightly broader. Due to its slower evolution, the B-band luminosity of SN 2008fz matches that of CSS121015 at about 30 d after maximum. The common feature of these light curves is that the rise to maximum is steeper than the post-maximum decline, which is linear without clear inflections. SN 2005gj is fainter by about two magnitudes than the other three SNe, and its light curve shows a steep rise and a much slower decline.

In canonical SNe IIn, the interaction with a relatively dense CSM sustains the luminosity of the SN until late phases, making the luminosity decline rate much slower than that expected from radioactive ^{56}Co decay (e.g. SN 1988Z; Turatto et al. 1993; Kiewe et al. 2012). In other SNe IIn, e.g. SNe 1994W (Sollerman, Cumming & Lundqvist 1998) and 2009kn (Kankare et al. 2012), the late-time decline is, to a first-order approximation, consistent with ^{56}Co decay. The fast early decline of H-rich SLSNe (SLSNe-II) is reminiscent of SNe IIL, some of which also show signatures of early interaction, e.g. SN 1994aj (Benetti et al. 1998), SN 1996L (Benetti et al. 1999) or of SNe IIn with fast photometric evolution, e.g. SN 1998S (Fassia et al. 2000, 2001; Leonard et al. 2000; Anupama, Sivarani & Pandey 2001).

6.2 Physical interpretation of the explosion

We have presented a photometric and spectroscopic study of CSS121015, which is among the most luminous SNe ever discovered. We have highlighted photometric similarities and differences with respect to a selected sample of SLSNe-II. As mentioned in Section 1, different scenarios have been proposed to explain the physical outputs of SLSNe, including pair-instability explosions that produce large Ni masses (e.g. Gal-Yam 2012); the energy deposited into an SN ejecta by a highly magnetic ($B \sim 5 \times 10^{14}$ G) neutron star spinning with an initial period of $P_i \sim 2$–20 ms (a magnetar; Kasen & Bildsten 2010); the accretion on to a compact remnant (Dexter & Kasen 2013); and the interaction of the ejecta with circumstellar material previously lost by the progenitor (Chevalier & Irwin 2011).

First, we explore the possibility that CSS121015 and similar objects may be powered by the spin-down of a magnetar, as proposed for SLSNe Ic (e.g. Inserra et al. 2013; Nicholl et al. 2013). For this goal, we fit the CSS121015 pseudo-bolometric/BB light curves using magnetar models as presented by Inserra et al. (2013) and Nicholl et al. (2013). The fit is initialized by comparing the observed light curve to a grid of magnetar-powered synthetic SN light curves. An exact fit is then found by χ^2 minimization.

In Fig. 8, we show reasonable fits to the pseudo-bolometric and BB-based bolometric curves of CSS121015 (Section 5) with magnetar models obtained adopting the following parameters. For the model fitting the pseudo-bolometric light curve, the input parameters were an ejected mass of $\sim 5.5\,\mathrm{M}_{\odot}$, a magnetic field of $B = 2.07 \times 10^{14}$ G and a neutron star with a period of $P_i \sim 1.99$ ms.

The BB bolometric light curve was instead fitted by a model obtained with an ejected mass of $\sim$5.6 M$_{\odot}$, magnetic field of $B = 1.42 \times 10^{14}$ G and a neutron star with a period of $P_i \sim 1.33$ ms (see Inserra et al. 2013 for details on the assumptions of the model). While the magnetar model fits the pseudo-bolometric light curve fairly well, the model fitting the BB bolometric curve provides a worse result, since there is a poor match of the curve before and around maximum light, where the model is somewhat broader than the extrapolated points. Remembering the uncertainties of the BB extrapolation, this fit is still quite reasonable.

Both models give a late-time light-curve tail (phase >100 d) with a higher luminosity than that inferred from the observed detection limits. This may be a consequence of the approximations adopted in the model (e.g. perhaps the magnetar energy is no longer fully trapped at late phases), or may be evidence that magnetar spin-down is not able to account for the full light curve of CSS121015. However, within the uncertainties of this kind of modelling, particularly in how the energy is deposited in the ejecta, a magnetar scenario cannot be excluded.

On the other hand, the narrow lines with decreasing fluxes seen in our spectra provide clear evidence of the presence of CSM lost by the progenitor before explosion. Therefore, it seems logical to investigate a scenario where the luminosity is powered by interaction of the SN ejecta with this CSM, and to verify consistency with the expected evolution of massive stars. Of course, it may also be possible that the narrow lines arise from a weak interaction with low-density CSM, while some other source, such as a magnetar, powers the continuum luminosity.

We begin assuming that the progenitor of CSS121015 was a restless, very massive star ($M > 50$ M$_{\odot}$), which during nuclear burning ejected several solar masses of material in distinct outbursts, resulting in a number of massive circumstellar shells (see e.g. Pastorello et al. 2010a; Foley et al. 2011; Smith et al. 2011). When the star experiences a subsequent major outburst, or the final core-collapse explosion, the fast expanding ejecta soon collide with the innermost massive shell, and a fraction of the kinetic energy of the ejecta is thermalized in the shell; this is the standard picture of ejecta–CSM interaction invoked for SNe IIn.

The shock occurs at the inner boundary of the massive, optically thick CSM shell, and in most cases will be observable only indirectly. In typical SNe IIn, the CSM is optically thin and the violent collision results in a number of phenomena, particularly strong X-ray and radio emission, strong optical emission lines with multiple components, including narrow features with velocity typical of the surrounding CSM, and intermediate features with FWHM of a few thousand km s^{-1}, arising from the shocked ejecta. The scenario can account for intermediate cases such as SN 2005gj, where the CSM is thin enough to show multiple-component emission lines, but not strong X-ray and radio emission (Aldering et al. 2006).

In the shock, kinetic energy is converted to radiation, and the shell is heated and accelerated. The luminosity rise time depends mainly on the radiation diffusion time-scale in the shell (for CSS121015, we find a relatively long $\sim$40 d rest-frame rise time), while the emerging spectrum is well fitted by a BB at high temperature. If the shell is initially at a large distance from the star, the early adiabatic losses after collision are small, and superluminous peak absolute magnitudes ($M < -21$) are possible (Quimby et al. 2011), provided the shell is sufficiently massive and opaque to efficiently thermalize a large fraction of the ejecta kinetic energy. This is the case applicable to CSS121015: at maximum light, we find that the still-opaque shell has a BB radius of $\sim$150 au (deduced from $\log L_{UBVRIz} \sim 44.5$ dex, assuming a BB temperature of $\sim$17 300 K, see Table 5). On the other hand, the radius determined from the BB-extrapolated luminosity (see Section 5) is $\sim$300 au which should be considered as an upper limit.

Similar opaque-shell models for SLSNe-II 2006tf and 2006gy had BB radii and temperatures of 300 au and 7800 K, and 320 au and $\sim$10 000 K, respectively (Smith & McCray 2007; Smith et al. 2008a). Perhaps more relevant is the comparison with SN 2008es owing to its observed similarities with CSS121015. Miller et al. (2009) found a temperature of $\sim$15 000 K and a radius of $\sim$260 au shortly after peak, very similar to our estimates for CSS121015.

At times longer than the diffusion time-scale, radiation leaks out at a significant rate from the cooling shell between the forward and reverse shocks. As the shell cools, instabilities in the shocked region lead to clumping (Smith et al. 2008b). The optical depth in the rarefied interclump regions drops rapidly, reducing the mean opacity, and finally allowing radiation from the shocked ejecta of the SN itself to escape (Smith et al. 2008a; Agnoletto 2010). About 70 d after maximum, the spectra start to be dominated by broad metal features (see Fig. 3), consistent with underlying Type Ic SN shocked ejecta. These features are relatively weak compared with that of a normal SN Ic, because in this case they appear superimposed on the extremely luminous BB emission from the pseudo-photosphere. These features are also very similar to those seen in SLSNe with no hydrogen in their spectra (SLSNe-Ic, cf. Section 6.3).

The BB radius increases constantly in time, as expected for an expanding and cooling pseudo-photosphere. It reaches an extension of about 450 au by the time of our last spectrum, or about 700 au in the case of BB extrapolation (see Table 5). Taking into account that the difference between the photospheric radius at the time of our last spectrum and the radius deduced at the epoch of our first spectrum is $\sim 4.5 \times 10^{15}$ cm (or $\sim 6.6 \times 10^{15}$ cm in the BB extrapolation), and that the time lapse between these two spectra is 70 d in the rest frame, we deduce for the pseudo-photosphere an average expansion velocity of $\sim$7400 km s^{-1}($\sim$10 600 km s^{-1} in the BB extrapolation). These numbers are comparable to the expansion velocity derived from the broad Hα emission.

In this scenario, the narrow-to-intermediate width Balmer emissions that are signatures of CSM interaction could be weak (as observed in CSS121015) or entirely absent, if the CSM shell is opaque and the shock encounters no further CSM at larger radii. As stated previously, the condition of a highly opaque shell must hold, in order to generate the observed continuum luminosity (Smith & McCray 2007). The fact that the spectrum remains featureless for a long time also demonstrates that there is a very high optical depth between the observer and the underlying SN shocked ejecta. An interesting question is whether there are regimes of density/temperature/opacity where the intermediate-width Balmer lines from the shocked region are absent, i.e. can this scenario also describe SLSNe-Ic? While this seems plausible, detailed spectral modelling is necessary for a confirmation.

The FWHM of the broad Balmer lines are not seen to decrease significantly with time (see Section 4.1). This is probably because, due to the $\gtrsim$30–40 d diffusion time in the shell, a great deal of CSM mass has been swept up by the forward shock before we observe any emission line. Deceleration of the shock likely does occur at early times, following the ejecta–CSM collision. However, by the time the transient becomes visible, the massive shell coasts at almost constant velocity, as it has been by now mostly swept up by the forward shock. The same phenomenon was observed in SN 2006tf and, according to Smith & McCray (2007), the fact that the shell does not slow down while it radiates $\gtrsim 10^{51}$ erg shows that it must comprise at least several solar masses.

The narrow components of the Balmer lines arise from an unshocked, low-velocity wind external to the dense shell (Smith et al. 2008a), which may be excited or ionized by radiation from the shell. The presence/density of this wind, perhaps along with the composition of the underlying ejecta (Type I versus Type II), is likely the origin of the spectral differences between CSS121015-like and 2006gy-like SLSNe-II, the last one displaying prominent, multicomponent Balmer lines (Smith & McCray 2007).

Since the radius deduced for CSS121015 exceeds that of typical red supergiants (Smith et al. 2001) by two orders of magnitude, we propose that the opaque CSM shell was ejected some time prior to the SN explosion and is not bound to the star. A similar model was suggested for SN 2008es for which the CSM mass was estimated between $\sim 5\,M_\odot$ (Miller et al. 2009) and $\sim 2.5-3\,M_\odot$ (Chatzopoulos et al. 2013).

Following the formalisms of Quimby et al. (2007) and Smith & McCray (2007) for the radiation emitted by a shocked, thermalized shell, the peak luminosity is $L \propto \frac{1}{2} M_{\rm sh} v_{\rm ph}^2 / t_{\rm max}$, where $M_{\rm sh}$ is the mass of the CSM shell, $v_{\rm ph}$ is the velocity of the pseudo-photosphere and $t_{\rm max}$ is the rise time of the bolometric light curve. If we assume that CSS121015 has a rise time ~1.9 times that of SN 2008es, a peak brighter by 0.12 dex and a comparable photospheric velocity (see Fig. 6), we estimate (with the above formula) a CSM mass of $\sim 8.5\,M_\odot$, where we have used a mass of $\sim 2.7\,M_\odot$ for the SN 2008es CSM shell (Chatzopoulos et al. 2013).

We can apply a consistency check on the energetics of our model. Smith & McCray (2007) note that, even with high efficiency in thermalizing the ejecta kinetic energy in the shell, momentum conservation tells us that the kinetic energy of the now-accelerated, shocked shell must be at least of the order of the thermal energy deposited. The thermal energy in the shell is eventually observed as radiation; integrating our pseudo-bolometric light curve implies that this is $\gtrsim 1.2 \times 10^{51}$ erg. Taking our estimated shell mass of $\sim 8.5\,M_\odot$ and velocity of $7400\,{\rm km\,s^{-1}}$, we estimate a kinetic energy of $\sim 4.7 \times 10^{51}$ erg, so the parameters we have derived do seem to be consistent. This also suggests that the explosion energy of the SN was $\gtrsim 5-6 \times 10^{51}$ erg.

With the derived mass, we can explain the relatively fast rise and decay observed for CSS121015, compared to other luminous, slowly evolving SNe (e.g. SN 2006gy; Ofek et al. 2007; Smith & McCray 2007; Agnoletto et al. 2009), since the radiation diffusion time for this SN is much shorter than in those events. If we assume that the mass comprising this shell was lost in a steady wind, we can estimate the mass-loss rate as follows: we take the BB radius at maximum light ($\sim 2 \times 10^{13}$ m) as a representative radius for the CSM shell (as the shell is optically thick, the photosphere should be near the outer edge, so this is a reasonable approximation), and a wind velocity of $10–100\,{\rm km\,s^{-1}}$ [where the upper limit corresponds to a typical luminous blue variable (LBV) wind], and find that the wind must have begun ~6–65 yr before explosion. The corresponding mass-loss rate is then $\sim 0.1–1\,M_\odot\,{\rm yr^{-1}}$, which is much larger than any known stellar wind. Normal wind-driven mass-loss therefore seems unlikely.

If instead, the mass-loss occurred in an outburst like those seen in SNe 1994aj (Benetti et al. 1998) and 1996L (Benetti et al. 1999), where the CSM shell had velocities of $\lesssim 800\,{\rm km\,s^{-1}}$ (a similar velocity is also deduced from the barely resolved CSS121015 narrow lines), then the impulsive mass ejection would have happened only one year before the core collapse. This violent mass-loss would have probably given rise to a pre-explosion optical transient, similar to those reported by Pastorello et al. (2007) for SN 2006jc, by Ofek et al. (2013) for SN 2010mc and by Fraser et al. (2013b) for SN 2011ht. The inspection of the pre-outburst light curve of CSS121015[7] does not show any strong activity within 7 yr before the explosion. However, the deepest limiting magnitudes of the pre-CSS121015 measurements are $\lesssim 20.6$, which corresponds to an absolute magnitude of $\lesssim -20.6$ mag. A massive ejection like those seen in SN 2006jc and proposed for SNe 1994aj and 1996L would have been well below the detection limit.

If we compare the luminosity upper limit at ~178–204 d (rest frame) with the bolometric luminosity of SN 1987A at a similar phase, we derive an upper limit of $\lesssim 2.5\,M_\odot$ for the ^{56}Ni mass ejected in the explosion. This value for the ^{56}Ni mass is still consistent with the lower limits of ^{56}Ni foreseen for some pair-instability scenario models (Whalen et al. 2013) in stars with initial masses between 150 and 200 $M_\odot$.

In summary, the observations of CSS121015 are consistent with a scenario in which the high luminosity arises from kinetic energy thermalized in the shock between the ejecta and a dense shell. This seems to require a circumstellar shell of a few solar masses, and therefore a massive star as its progenitor. The opaque shell implies that we do not get a direct view of the SN ejecta until approximately 60 d (rest frame) after explosion. The lines that eventually appear are reminiscent of SLSNe-Ic. For the explosion mechanism, there is no evidence to support a pair-instability SN with an high production of ^{56}Ni mass, while a pair instability with a low ^{56}Ni production explosion (Heger et al. 2003; Yoon, Dierks & Langer 2012) can still be possible, but it would fail to explain the peak luminosity. On the other hand, an energetic core-collapse explosion from a stripped-envelope progenitor could be the more natural candidate for the explosion mechanism.

6.3 H-poor SLSNe (SLSNe-Ic) in the context of CSS121015

We argued that the reprocessing of kinetic energy into radiation via ejecta–CSM interaction would satisfactorily explain the properties of SLSNe-II. However, whether this mechanism may also explain the behaviour of very luminous H-poor events is still a subject of debate. Thermonuclear explosion, triggered by pair production in an extremely massive star, has been proposed to explain the H-poor SLSN 2007bi (Gal-Yam et al. 2009, but see Dessart et al. 2012), whose late-time light curve has a slope which is consistent with ^{56}Co decay. Nonetheless, a more canonical core collapse, with the ejection of a relatively large amount of ^{56}Ni, may reproduce equally well the high luminosity observed in this SN and its overall early-time spectrophotometric properties (Moriya et al. 2010; Young et al. 2010).

Another group of SLSNe-Ic shows relatively narrow light curves, with a linear decline at late times, much faster than that expected from the ^{56}Co decay (Barbary et al. 2009; Pastorello et al. 2010b; Chomiuk et al. 2011; Quimby et al. 2011; Leloudas et al. 2012; Chornock et al. 2013; Inserra et al. 2013; Lunnan et al. 2013). This implies that these events cannot be powered by large masses of radioactive material. Indeed, based on data of two recent SNe spectroscopically similar to SN 2007bi, Nicholl et al. (2013, see also McCrum et al. 2014) argued that they that are not consistent with very massive, nickel-rich ejecta.

Here we want to emphasize the similarity between CSS121015 and some SLSNe-Ic. In this view, it is interesting to note that most SLSNe-II are observed in similar host dwarf galaxies as SLSNe-Ic

[7] http://voeventnet.caltech.edu/feeds/ATEL/CRTS/1210151120044133047.atel.html

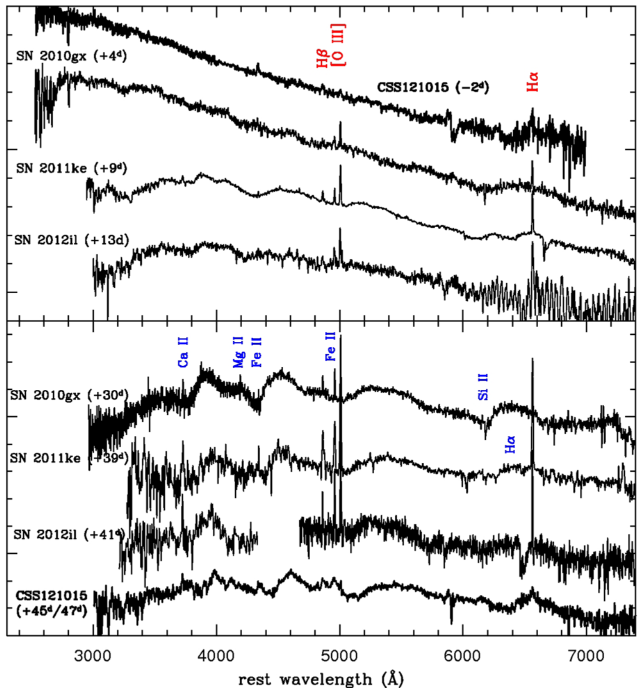

Figure 10. Rest-frame comparison between CSS121015 and SLSNe-Ic spectra at two phases: around the maximum light (top) and about 1–1.5 months after the maximum (bottom). The spectra are very similar bluewards of 6000 Å. The major difference is the Hα region, which in SLSNe-Ic is probably dominated by the Si II 6355 Å transition. The expansion velocities seem to be similar in the entire sample. Line identifications are taken from Pastorello et al. (2010b).

(Neill et al. 2011), although SN 2006gy exploded in NGC 1260 – a much more massive, redder galaxy.

To emphasize the similarity, we constructed the quasi-bolometric light curves for a selected sample of H-poor SLSNe: SN 2010gx (Pastorello et al. 2010b), SN 2011ke and SN 2012il (Inserra et al. 2013) and compared them with that of CSS121015, after correction for time dilatation, in Fig. 9. All pseudo-bolometric light curves were computed following the same prescriptions as reported in Section 5.

In Fig. 10, we compare the spectra at around the maximum light in the top panel, while spectra at phases of about 1–1.5 months after maximum are compared in the bottom panel. The phases have been computed after correcting for time dilation. A suggestive degree of similarity is seen – particularly at 1–1.5 months, when a number of common lines are detected, including Ca II, Mg II and Fe II. The overall spectral shape is also surprisingly similar in our sample spectra, with the only difference lying in the broad feature at 6300–6600 Å. This has been identified as either Hα or Si II λ6355 Å, depending on the case. In some objects (e.g. SN 2011ke), the identification of the broad feature may be disputable, with Hα probably being a more solid identification for this SN. However, while the broad Hα has strengthened in CSS121015 from phase +38 to +86 d, the corresponding feature in SN 2011ke has weakened with time.

On the other hand, the spectra around maximum light (top panel) may show significant differences, as all of the H-poor SLSNe exhibit broad lines a few days either side of maximum, while CSS121015 shows little sign of such features until at least two weeks later. The persistent featureless spectrum of CSS121015 is consistent with a highly optically thick shell, and is further evidence in favour of circumstellar interaction. But the appearance of broad (SN?) lines early in the evolution of SLSNe Ic [Quimby et al. (2011) and Nicholl et al. (2013) have found broad lines two to three weeks before maximum light] may be difficult to reconcile with a model where opaque shells surround the SNe: these shells should conceal any spectral lines originating in the ejecta, until the CSM has had time to cool radiatively and decrease its optical depth. However, since many factors (e.g. CSM clumping) affect the emergent spectrum and time-scales in a scenario as complex as ejecta–CSM interaction, it is difficult to say how strong a constraint this is without detailed spectral models.

Regardless, the overall spectral similarity suggests that the underlying ejecta composition is consistent across our sample, i.e. the SNe are probably all from stripped-envelope progenitors. If all these SNe were powered by interaction, the presence or absence of H in the spectrum could be simply a consequence of different shell properties – namely in SLSNe-Ic, the CSM may be H-deficient. We note that all SLSNe-Ic develop Type Ic features on much longer time-scales than normal SNe Ic (Pastorello et al. 2010b), and the presence of an initially highly opaque shell could potentially explain the cause.

Since CSS121015 seems to be largely consistent with the ejecta–CSM interaction scenario, we propose that this should be considered as an efficient mechanism for generating the enormous luminosities observed in many SLSNe, independent of the composition (H-rich or -deficient) of their outer stellar envelopes. However, we note that other SLSNe-Ic, including the SN 2007bi-like group, have quite different spectrophotometric properties. Therefore, it is premature to claim a common powering mechanism for *all SLSNe*.

The diversity in the spectra between different subtypes (SLSNe-Ic and SLSNe-II, CSS121015-like and 2006gy-like) may perhaps be explained in terms of differences in the structure and hydrogen content of their circumstellar cocoons.

A thorough comparison between different powering mechanisms in SLSNe II and Ic will be the topic of an in-depth, forthcoming investigation (Nicholl et al., in preparation).

7 CONCLUSIONS

We have presented extensive data for CSS121015, covering over 200 d (rest frame) of evolution. The collected observations, which consist of *UBVRIgriz* photometry and low-resolution optical spectroscopy, make this one of the most comprehensive data sets for an SLSN.

The analysis of the observations of CSS121015 shows that this is among the most luminous SNe ever discovered. Its photometric evolution is characterized by a relatively fast rise to maximum (∼40 d in the SN rest frame), and by a post-maximum decline typical of SNe II-Linear. Its light curve shows no sign of a break to an exponential tail.

Compared to others SLSNe, the spectral evolution is relatively fast after maximum. The first available spectrum shows a very hot (T_{BB} ∼ 17 700 K) and featureless continuum. The continuum cools down quickly after maximum, and the spectra show the first broad features two weeks after maximum (in the rest frame). A broad Hα line is first detected at ∼+ 39 d (rest frame). Narrow, barely resolved Balmer and [O III] 5007 Å lines with decreasing flux are visible along the entire spectral evolution, and were gone in the spectra of the CSS121015 host taken about one year after the explosion.

The spectra are very similar to other SLSNe-II and also to SN 2005gj, previously classified as SN IIa (Ia interacting with H-rich CSM).

Although our analysis does not rule out magnetar spin-down as a viable mechanism to explain the enormous luminosity of SLSNe, our preferred model to explain CSS121015, and perhaps many other SLSNe (with and without H), is the interaction of the ejecta with a massive, extended, opaque shell, lost by the progenitor decades before the final explosion, which could either be an energetic core collapse or a pair instability with a low ^{56}Ni production explosion.

ACKNOWLEDGEMENTS

We thank the anonymous referee for very useful comments and suggestions.

SB, EC, AP, LT and MT are partially supported by the PRIN-INAF 2011 with the project Transient Universe: from ESO Large to PESSTOÓ. Research leading to these results has received funding from the European Research Council under the European Union's Seventh Framework Programme (FP7/2007-2013)/ERC Grant agreement no. [291222] (PI: SJS) and EU/FP7-ERC grant no. [307260] (PI: AG-Y). AG-Y is also supported by 'The Quantum UniverseÓ I-Core programme by the Israeli Committee for planning and funding and the ISF, a GIF grant, and the Kimmel award'. NER and AMG acknowledge financial support by the MICINN grant AYA2011-24704/ESP, and by the ESF EUROCORES Program EuroGENESIS (MINECO grants EUI2009-04170). NER acknowledges the support from the European Union Seventh Framework Programme (FP7/2007-2013) under grant agreement no. 267251. The CRTS survey is supported by the US National Science Foundation under grant AST-1313422.

This work is partially based on observations collected at (1) the European Organisation for Astronomical Research in the Southern hemisphere, Chile as part of PESSTO, (the PESSTO survey) ESO programme 188.D-3003; (2) the Copernico 1.82 m Telescope operated by INAF – Osservatorio Astronomico di Padova at Asiago; (3) the 3.6 m Italian Telescopio Nazionale Galileo operated by the Fundación Galileo Galilei – INAF on the island of La Palma; (4) the 4.3 m William Herschel Telescope operated by the Isaac Newton Group of Telescope; (5) the Gran Telescopio Canarias (GTC), installed in the Spanish Observatorio del Roque de los Muchachos of the Instituto de Astrof'sica de Canarias, in the island of La Palma; (6) the Liverpool Telescope, which is operated on the island of La Palma by Liverpool John Moores University in the Spanish Observatorio del Roque de los Muchachos of the Instituto de Astrofisica de Canarias with financial support from the UK Science and Technology Facilities Council; (6) the Faulkes Telescope Project, which is an educational and research arm of the Las Cumbres Observatory Global Telescope Network (LCOGTN); (7) the Large Binocular Telescope (LBT), which is an international collaboration among institutions in the United States, Italy and Germany. The LBT Corporation partners are the University of Arizona on behalf of the Arizona university system; Istituto Nazionale di Astrofisica, Italy; LBT Beteiligungsgesellschaft, Germany, representing the Max Planck Society, the Astrophysical Institute Potsdam and Heidelberg University; the Ohio State University; the Research Corporation, on behalf of the University of Notre Dame, University of Minnesota and University of Virginia.

This research has made use of the NASA/IPAC Extragalactic Database (NED) which is operated by the Jet Propulsion Laboratory, California Institute of Technology, under contract with the National Aeronautics and Space Administration. We thank R. Kotak for taking the WHT+intermediate dispersion spectrograph and imaging system (ISIS) spectrum of 2012 November 20.

REFERENCES

Ade P. A. R. et al., 2013, A&A, preprint (arXiv:1303.5076)
Agnoletto I., 2010, PhD thesis, Padua Univ.
Agnoletto I. et al., 2009, ApJ, 691, 1348
Aldering G. et al., 2006, ApJ, 650, 510
Anupama G. C., Sivarani T., Pandey G., 2001, A&A, 367, 506
Arcavi I. et al., 2012, ApJ, 756, L30
Baltay C. et al., 2013, PASP, 125, 683
Barbary K. et al., 2009, ApJ, 690, 1358
Ben-Ami S. et al., 2014, ApJ, 785, 37
Benetti S., Cappellaro E., Danziger I. J., Turatto M., Patat F., della Valle M., 1998, MNRAS, 294, 448
Benetti S., Turatto M., Cappellaro E., Danziger I. J., Mazzali P. A., 1999, MNRAS, 305, 811
Benetti S., Cappellaro E., Turatto M., Taubenberger S., Harutyunyan A., Valenti S., 2006, ApJ, 653, L129
Blinnikov S. I., Sorokina E. I., 2010, preprint (arXiv:1009.4353)
Chatzopoulos E., Wheeler J. C., Vinko J., Horvath Z. L., Nagy A., 2013, ApJ, 773, 76
Chevalier R. A., Irwin C. M., 2011, ApJ, 729, L6
Chomiuk L. et al., 2011, ApJ, 743, 114
Chornock R. et al., 2013, ApJ, 767, 162
Cooke J. et al., 2012, Nature, 491, 228
Dessart L., Hillier D. J., Waldman R., Livne E., Blondin S., 2012, MNRAS, 426, L76
Dexter J., Kasen D., 2013, ApJ, 772, 30
Drake R. P., Kuranz C. C., Miles A. R., Muthsam H. J., Plewa T., 2009, Phys. Plasmas, 16, 041004
Drake A. J. et al., 2010, ApJ, 718, L127
Drake A. J. et al., 2012, Astron. Telegram, 4498, 1
Eisenstein D. J. et al., 2011, AJ, 142, 72
Fassia A. et al., 2000, MNRAS, 318, 1093
Fassia A. et al., 2001, MNRAS, 325, 907
Foley R. J., Berger E., Fox O., Levesque E. M., Challis P. J., Ivans I. I., Rhoads J. E., Soderberg A. M., 2011, ApJ, 732, 32
Fraser M. et al., 2013a, MNRAS, 433, 1312
Fraser M. et al., 2013b, ApJ, 779, L8
Gal-Yam A., 2012, Science, 337, 927
Gal-Yam A. et al., 2009, Nature, 462, 624
Gezari S. et al., 2009, ApJ, 690, 1313
Ginzburg S., Balberg S., 2012, ApJ, 757, 178
Harutyunyan A. H. et al., 2008, A&A, 488, 383
Heger A., Fryer C. L., Woosley S. E., Langer N., Hartmann D. H., 2003, ApJ, 591, 288
Howell D. A. et al., 2013, ApJ, 779, 98
Inserra C. et al., 2013, ApJ, 770, 128
Inserra C. et al., 2014, MNRAS, 437, L51
Kankare E. et al., 2012, MNRAS, 424, 855
Kasen D., Bildsten L., 2010, ApJ, 717, 245
Kiewe M. et al., 2012, ApJ, 744, 10
Kim A., Goobar A., Perlmutter S., 1996, PASP, 108, 190
Landolt A. U., 1992, AJ, 104, 340
Law N. M. et al., 2009, PASP, 121, 1395
Leloudas G. et al., 2012, A&A, 541, A129
Leonard D. C., Filippenko A. V., Barth A. J., Matheson T., 2000, ApJ, 536, 239
Lunnan R. et al., 2013, ApJ, 771, 97
Margutti R. et al., 2014, ApJ, 780, 21
Mauerhan J. C. et al., 2013, MNRAS, 430, 1801
Maund J. R. et al., 2006, MNRAS, 369, 390
McCrum M. et al., 2014, MNRAS, 437, 656
Miller A. A. et al., 2009, ApJ, 690, 1303

Moriya T., Tominaga N., Tanaka M., Maeda K., Nomoto K., 2010, ApJ, 717, L83
Moriya T., Blinnikov S. I., Tominaga N., Yoshida N., Tanaka M., Maeda K., Nomoto K., 2013a, MNRAS, 428, 1020
Moriya T., Blinnikov S. I., Baklanov P. V., Sorokina E. I., Dolgov A. D., 2013b, MNRAS, 430, 1402
Moriya T., Maeda K., Taddia F., Sollerman J., Blinnikov S. I., Sorokina E. I., 2013c, MNRAS, 435, 1520
Neill J. D. et al., 2011, ApJ, 727, 15
Nicholl M. et al., 2013, Nature, 502, 346
Ofek E. O. et al., 2007, ApJ, 659, L13
Ofek E. O. et al., 2013, Nature, 494, 65
Pastorello A. et al., 2007, Nature, 447, 829
Pastorello A. et al., 2010a, MNRAS, 408, 181
Pastorello A. et al., 2010b, ApJ, 724, L16
Pastorello A. et al., 2013, ApJ, 767, 1
Patat F., Barbon R., Cappellaro E., Turatto M., 1994, A&A, 282, 731
Poznanski D., Prochaska J. X., Bloom J. S., 2012, MNRAS, 426, 1465
Prieto J. L. et al., 2007, preprint (arXiv:0706.4088)
Quimby R. M., Aldering G., Wheeler J. C., Höflich P., Akerlof C. W., Rykoff E. S., 2007, ApJ, 668, L99
Quimby R. M. et al., 2011, Nature, 474, 487
Quimby R. M., Yuan F., Akerlof C., Wheeler J. C., 2013, MNRAS, 431, 912
Schlafly E. F., Finkbeiner D. P., 2011, ApJ, 737, 103
Smith N., McCray R., 2007, ApJ, 671, L17
Smith N., Humphreys R. M., Davidson K., Gehrz R. D., Schuster M. T., Krautter J., 2001, AJ, 121, 1111
Smith N. et al., 2007, ApJ, 666, 1116
Smith N. et al., 2008a, ApJ, 686, 485
Smith N., Chornock R., Li W., Ganeshalingam M., Silverman J. M., Foley R. J., Filippenko A. V., Barth A. J., 2008b, ApJ, 686, 467
Smith N., Li W., Silverman J. M., Ganeshalingam M., Filippenko A. V., 2011, MNRAS, 415, 773
Tomasella L., Benetti S., Pastorello A., Cappellaro E., Turatto M., Harutyunyan A., 2012, Astron. Telegram, 4512, 1
Tonry J. L. et al., 2012, ApJ, 745, 42
Trundle C., Kotak R., Vink J. S., Meikle W. P. S., 2008, A&A, 483, L47
Turatto M., Cappellaro E., Danziger I. J., Benetti S., Gouiffes C., della Valle M., 1993, MNRAS, 262, 128
Turatto M., Benetti S., Cappellaro E., 2003, in Hillebrandt W., Leibundgut B., eds, Proc. ESO/MPA/MPE Workshop, From Twilight to Highlight: The Physics of Supernovae. Springer-Verlag, Berlin, p. 200
Van Dyk S. D., Peng C. Y., King J. Y., Filippenko A. V., Treffers R. R., Li W., Richmond M. W., 2000, PASP, 112, 1532
Whalen D. J., Joggerst C. C., Fryer C. L., Stiavelli M., Heger A., Holz D. E., 2013, ApJ, 768, 95
Woosley S. E., 2010, ApJ, 719, L204
Yoon S.-C., Dierks A., Langer N., 2012, A&A, 542, A113
Young D. R. et al., 2010, A&A, 512, 70
Sollerman J., Cumming R. J., Lundqvist P., 1998, ApJ, 493, 933

This paper has been typeset from a TEX/LATEX file prepared by the author.